Progress In Electromagnetics Research B, Vol. 41, 1–22, 2012

DETERMINATION OF CLOSED-FORM EXPRESSIONS FOR RAYLEIGH SCATTERING OF POLARIZED LIGHT FROM ADSORBED PARTICLES ON OR BELOW A SUBSTRATE

R. A. Simpkin*

Industrial Research Limited, 24 Balfour Road, Parnell, Auckland 1140, New Zealand

Abstract—An integral equation formulation describing the scattered field from a distribution of optically small Rayleigh objects of arbitrary shape adsorbed onto a planar dielectric substrate is presented. When certain approximations are introduced concerning the scatterers' permittivity contrast and small size compared to the wavelength, simple closed-form expressions are obtained for the ellipticity ratio and reflectivity which can be readily related to the surface coverage and average height of the surface layer. The formulation is an alternative to thin-island film theory often used to describe electromagnetic scattering from such configurations. Results derived from the integral equation model are compared with previously published measurements of ellipticity ratio and reflectivity and are found to be in good agreement with observation.

1. INTRODUCTION

An understanding of the optical properties of adsorbed particles on a supporting substrate is an important phenomenon to analytical techniques such as ellipsometry and reflectometry which have found widespread use in biological, chemical and industrial applications. For adsorbed layers consisting of biological agents such as proteins, the size of the particles is of the order of tens of nanometres; an order of magnitude smaller than the wavelength of incident light used in optical measurements (typically 633 nm in free-space, 475 nm in water). The small optical thickness of such adsorbed particles, so-called Rayleigh

Received 30 March 2012, Accepted 28 April 2012, Scheduled 15 May 2012

* Corresponding author: Ray Simpkin (r.simpkin@irl.cri.nz).

objects, discounts the possibility of direct microscopic observation. Only the small perturbations from pure Fresnel reflection on quantities such as the ellipticity ratio and reflectivity near the Brewster angle enable measurements of the adsorbed layer's properties to be made.

Optical scattering from a distribution of Rayleigh objects on a planar substrate has been analysed by a number of previous researchers. Of particular importance is the thin-island film theory proposed by Bedeaux and Vlieger [1, 2], which derives expressions for excess surface polarizabilities perpendicular and parallel to the surface. These expressions are based on the scattering properties of spherical particles to varying orders of interaction with the substrate, and account for the perturbing effect of the adsorbed layer. An exact formulation for a single spherical scatterer on a dielectric substrate was presented by Bobbert and Vlieger [3] based on a Mie series expansion and plane-wave spectral formulation. The same authors, in collaboration with Greef, extended this analysis to sparse distributions of spherical particles [4]. A similar single-sphere analysis was performed by Videen for the case of a sphere behind a substrate [5]. Comparisons between theoretical predictions and measured data for Rayleigh objects placed on or below a substrate are relatively uncommon in the literature. The work of van Duijvenbode and Koper [6] is one of the few publications containing such a comparison for ellipticity ratio and reflectivity measurements carried out in the vicinity of the Brewster Angle. The measured data reported in [6] for small latex spheres of known radius and refractive index is used in this paper for comparison with theoretical predictions. The review article of Moreno et al. [7] describes theoretical and experimental results for the case of optical scattering from metallic particles on a substrate. However, the research described in [7] relates to the case for which the particle size is comparable to the wavelength of light used and, as such, does not constitute Rayleigh scattering.

An alternative formulation is presented here for the scattering from adsorbed particles on a substrate. This utilises the superposition of volume and surface integrals based on the rigorous scattering theory due to Stratton and Chu [8]. It will be shown that when this formulation is applied to objects small compared to the wavelength of incident light (the defining property of a Rayleigh object), the dependence on particle shape vanishes. In addition, applying the approximation that the permittivity contrast between scatterer and host medium is small (the so-called Born Approximation), results in integrals for the scattered field that can be easily evaluated to give simple closed-form expressions involving the surface coverage and effective height of the adsorbed layer.

2. THEORY

2.1. Object Above Substrate

Figure 1 shows a Rayleigh object of arbitrary shape in close contact with a planar dielectric substrate illuminated by a plane wave propagating in the same host medium in which the scatterer resides. This case is typical of adsorbed particles in an aqueous medium above an opaque substrate material such as silicon or carbon. A single scatterer is shown here for clarity but the analysis can be applied to multiple scatterers distributed over the substrate by employing superposition. The case for which the scatterer lies beneath the interface between host medium and substrate will also be analysed in this paper. This case is typical of adsorbed particles in an aqueous medium beneath a transparent substrate such as glass.

From the electromagnetic scattering theory developed by Stratton & Chu [8], the scattered electric field at a point, P, denoted by $\mathbf{E}_{\text{scat}}(P)$, lying within the host medium can be determined from the sum of the following two terms, each of which can be expressed as an integral:

$$\mathbf{E}_{\text{scat}}(P) = \mathbf{E}^{V}_{\text{scat}} + \mathbf{E}^{S}_{\text{scat}} \tag{1}$$

where in (1)

$$\mathbf{E}^{V}_{\text{scat}} = \frac{-j}{4\pi\omega\varepsilon_0\varepsilon_1}\int_V \left[(\mathbf{J}\cdot\nabla)\nabla\phi + k_1^2\mathbf{J}\phi\right]dV \tag{2}$$

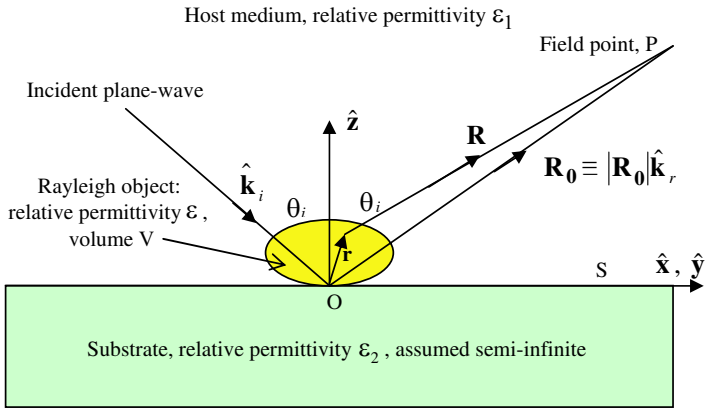

Figure 1. Geometry of a Rayleigh object above a substrate.

$$\mathbf{E}^S_{\text{scat}} = \frac{-j}{4\pi\omega\varepsilon_0\varepsilon_1}\iint_S \left[(\mathbf{J}_s\cdot\nabla)\,\nabla\phi + k_1^2\mathbf{J}_s\phi - j\omega\varepsilon_0\varepsilon_1\mathbf{M}_s\times\nabla\phi\right]dS \quad (3)$$

In the above equations, $j = \sqrt{-1}$ and harmonic time-dependence is assumed with the form $e^{j\omega t}$. This factor is suppressed from the above and all subsequent expressions.

Equation (2) represents the contribution to the scattered field from the Rayleigh object. This has the form of an integral over the volume V involving the induced polarization current density $\mathbf{J}$.

Equation (3) represents the contribution to the scattered field from the planar interface at $z = 0$ between the host medium and substrate. This takes the form of a surface integral over $\mathbf{S}$ involving equivalent electric and magnetic currents $\mathbf{J}_s$ and $\mathbf{M}_s$, respectively. Note that the surface $\mathbf{S}$ consists of the entire substrate surface — both covered and exposed parts. Also, it is assumed that $\mathbf{S}$ is sufficiently large compared to the wavelength to be regarded as infinite in lateral extent a condition that is readily satisfied in practice. With the exception of the substrate-host medium interface, the remaining bounding surfaces of the host medium are assumed to be far enough away from the substrate as to be at infinity. The scattered electric field on these bounding surfaces therefore vanishes in this case due to the radiation conditions at infinity, leaving only the substrate surface $\mathbf{S}$ contributing to the scattered field at the interior field point P.

Other terms in Equations (2) and (3), and in the figure, are defined as follows:

$\phi = \frac{\exp(-jk_1R)}{R}$ = Scalar Green's function for the host medium.

k_1 = Propagation constant for the host medium (radians per metre).

$\mathbf{R}$ = Position vector from source point to field point, P.

$R = |\mathbf{R}|$ = Distance from source point to field point, P.

$\mathbf{R}_0$ = Position vector from the coordinate origin to the field point, P.

$\mathbf{r}$ = Position vector from coordinate origin to the source point.

ε_1 = Complex relative permittivity of host medium.

ε_2 = Complex relative permittivity of substrate.

ε = Complex relative permittivity of Rayleigh object.

ε_0 = Permittivity of free space = $8.854 \times 10^{-12}\,\text{Fm}^{-1}$.

ω = Angular frequency (radians per second).

$\hat{\mathbf{k}}_i$ = Unit vector defining incident field propagation direction.

$\hat{\mathbf{k}}_r$ = Unit vector defining reflected field propagation direction.

Considering first the volume integral in (2), the polarization current density $\mathbf{J}$ is defined in terms of the permittivity contrast between host medium and Rayleigh object and the total interior electric field $\mathbf{E}_{\text{total}}$ as follows:

$$\mathbf{J} = j\omega\varepsilon_0 (\varepsilon - \varepsilon_1) \mathbf{E}_{\text{total}} \tag{4}$$

For a dielectric object that is much smaller in size compared to the wavelength in the host and object media, the Born approximation can be used to define the electric field inside the object. That is, the interior electric field $\mathbf{E}_{\text{total}}$ can be approximated by the field that exists over the volume V *in the absence of the object*. By way of a typical example, for a free-space wavelength of 633 nm, the wavelength in a host medium of water (refractive index, $n_1 = 1.333$) is 475 nm. That within a protein-based Rayleigh object (refractive index, $n = 1.5$) is 422 nm. Thus, an object 40 nm in diameter is approximately 1/10th of a wavelength across, small enough to be considered a Rayleigh object. In addition, the permittivity contrast is $\varepsilon - \varepsilon_1 = n^2 - n_1^2 = 0.47$ which is small enough for application of the Born Approximation.

Therefore, in (4), the electric field $\mathbf{E}_{\text{total}}$ is well-approximated by the sum of the incident field plus that specularly reflected from the planar substrate *with the Rayleigh object removed*. That is:

$$\mathbf{E}_{\text{total}} \cong E_0\phi_{\text{inc}} (\cos\gamma\hat{\mathbf{s}} + \sin\gamma\hat{\mathbf{p}}_i) + E_0\phi_{\text{ref}} \left(r_s^{12}\cos\gamma\hat{\mathbf{s}} + r_p^{12}\sin\gamma\hat{\mathbf{p}}_r\right) \tag{5}$$

where in (5):

γ = Polarization angle
= 0 for perpendicular polarization
= $\pi/2$ for parallel polarization.

$\hat{\mathbf{s}}$ = Unit vector perpendicular to the plane of incidence.

$\hat{\mathbf{p}}_i$ = Unit vector parallel to the plane of incidence for the incident field
= $\hat{\mathbf{k}}_i \times \hat{\mathbf{s}}$

$\hat{\mathbf{p}}_r$ = Unit vector parallel to the plane of incidence for the reflected field
= $-\hat{\mathbf{k}}_r \times \hat{\mathbf{s}}$

r_s^{12} = Fresnel reflection coefficient for perpendicular polarization for an incident plane wave in medium '1'.

r_p^{12} = Fresnel reflection coefficient for parallel polarization for an incident plane wave in medium '1'.

E_0 = Amplitude of the incident electric field.

ϕ_{inc} = Phase factor for the incident plane-wave.

ϕ_{ref} = Phase factor for the reflected plane-wave.

The plane-wave phase factors can be written in terms of the Cartesian coordinates x,y,z and the spherical polar angles θ_i, ϕ_i as follows:

$$\begin{aligned} \phi_{\text{inc}} &= \phi_t \exp\left(+jk_1 z\cos\theta_i\right) \\ \phi_{\text{ref}} &= \phi_t \exp\left(-jk_1 z\cos\theta_i\right) \end{aligned} \tag{6}$$

where the transverse phase factor ϕ_t is defined as:

$$\phi_t = \exp\left(-jk_1 x\sin\theta_i\cos\phi_i\right)\exp\left(-jk_1 y\sin\theta_i\sin\phi_i\right) \tag{7}$$

The angle of incidence is defined by θ_i.

Returning to the volume integrand in (2), the vector differential operator ∇ operates on the source coordinates that define a point within the Rayleigh scatterer relative to the origin O. Performing the necessary vector differentiations and using (4) for the polarization current density gives the following form for the volume integral contribution to the scattered field:

$$\begin{aligned} \mathbf{E}_{\text{scat}}^{V} &= \frac{-j}{4\pi\omega\varepsilon_0\varepsilon_1}\int_V \left[\left(\mathbf{J}\cdot\nabla\right)\nabla\phi + k_1^2\mathbf{J}\phi\right]dV \\ &= \frac{k_0^2}{4\pi}\left(\varepsilon-\varepsilon_1\right)\int_V \left[a\mathbf{E}_{\text{total}} + b\left(\mathbf{E}_{\text{total}}\cdot\hat{\mathbf{R}}\right)\hat{\mathbf{R}}\right]\phi\, dV \end{aligned} \tag{8}$$

where in (8)

k_0 = Propagation constant for free space.

$\hat{\mathbf{R}}$ = Unit vector parallel to the vector $\mathbf{R}$.

$$a = 1 - \frac{j}{k_1 R} - \frac{1}{(k_1 R)^2} \qquad b = -1 + \frac{3j}{k_1 R} + \frac{3}{(k_1 R)^2}$$

When $k_1 R \gg 1$, as is usually the case in practice, the above factors can be approximated as $a \approx 1$ and $b \approx -1$. In addition, $\hat{\mathbf{R}} \approx \hat{\mathbf{R}}_{\mathbf{0}}$ the unit vector parallel to $\mathbf{R}_0$. Therefore, under these far-field conditions (8) becomes:

$$\mathbf{E}_{\text{scat}}^{V} = \frac{k_0^2}{4\pi}\left(\varepsilon-\varepsilon_1\right)\int_V \left[\mathbf{E}_{\text{total}} - \left(\mathbf{E}_{\text{total}}\cdot\hat{\mathbf{R}}_0\right)\hat{\mathbf{R}}_0\right]\phi\, dV \tag{9}$$

We now consider the individual cases for perpendicular and parallel polarized incidence. For perpendicular polarization ($\gamma = 0$) Equation (9) becomes

$$E_s^V = \mathbf{E}_{\text{scat}}^{V}\cdot\hat{\mathbf{s}} = \frac{k_0^2}{4\pi}\left(\varepsilon-\varepsilon_1\right)\int_V \left[\mathbf{E}_{\text{total}}\cdot\hat{\mathbf{s}} - \left(\mathbf{E}_{\text{total}}\cdot\hat{\mathbf{R}}_0\right)\hat{\mathbf{R}}_0\cdot\hat{\mathbf{s}}\right]\phi\, dV$$

In the above, the scalar product $\hat{\mathbf{R}}_0 \cdot \hat{\mathbf{s}}$ is always zero since $\hat{\mathbf{R}}_0$ and $\hat{\mathbf{s}}$ are orthogonal vectors. Therefore, the only non-zero term in the above integrand is $\mathbf{E}_{\text{total}} \cdot \hat{\mathbf{s}} = E_0 \left(\phi_{\text{inc}} + r_s \phi_{\text{ref}}\right)$. This latter expression comes from the result of Equation (5).

Using the expressions in (6) and (7) for the plane-wave phase factors then gives the following result:

$$E_s^V = \mathbf{E}_{\text{scat}}^V \cdot \hat{\mathbf{s}} = \frac{k_0^2}{4\pi} \left(\varepsilon - \varepsilon_1\right) E_0 \int\limits_V \left(e^{j\beta z} + r_s^{12} e^{-j\beta z}\right) \phi_t \phi \, dV \qquad (10)$$

where in (10) $\beta = k_1 \cos\theta_i$, the z-component of the incident propagation vector in the host medium.

Similarly, for parallel polarization ($\gamma = \pi/2$), the volume integral contribution to the scattered field is given by:

$$E_p^V = \mathbf{E}_{\text{scat}}^V \cdot \hat{\mathbf{p}}_r = \frac{k_0^2}{4\pi} (\varepsilon - \varepsilon_1) \int\limits_V \left[\mathbf{E}_{\text{total}} \cdot \hat{\mathbf{p}}_r - \left(\mathbf{E}_{\text{total}} \cdot \hat{\mathbf{R}}_0\right) \hat{\mathbf{R}}_0 \cdot \hat{\mathbf{p}}_r\right] \phi \, dV$$

In the above, the scalar product $\hat{\mathbf{R}}_0 \cdot \hat{\mathbf{p}}_r$ is always zero since $\hat{\mathbf{R}}_0$ and $\hat{\mathbf{p}}_r$ are orthogonal vectors. Therefore, the only non-zero term in the above integrand is (using (5))

$$\mathbf{E} \cdot \hat{\mathbf{p}}_r = E_0 \left(\phi_{\text{inc}} \hat{\mathbf{p}}_r \cdot \hat{\mathbf{p}}_i + r_p^{12} \phi_{\text{ref}}\right) = E_0 \left(\phi_{\text{inc}} \cos 2\theta_i + r_p^{12} \phi_{\text{ref}}\right)$$

where the factor $\cos 2\theta_i$ arises from the scalar product $\hat{\mathbf{p}}_r \cdot \hat{\mathbf{p}}_i$. Therefore, we obtain the following expression for parallel polarization:

$$E_p^V = \mathbf{E}_{\text{scat}}^V \cdot \hat{\mathbf{p}}_r = \frac{k_0^2}{4\pi} (\varepsilon - \varepsilon_1) E_0 \int\limits_V \left(\cos 2\theta_i e^{j\beta z} + r_p^{12} e^{-j\beta z}\right) \phi_t \phi \, dV \quad (11)$$

In the expressions given in (10) and (11), it can be seen that the integrand is a sum of two terms. The first term in each case, proportional to the phase factor $e^{j\beta z}$, is that due to the relevant component of the incident electric field lying within the volume of the Rayleigh scatterer. The remaining term in each case, proportional to the phase factor $e^{-j\beta z}$, is that due to the Fresnel-reflected field from the substrate that impinges upon the volume of the Rayleigh scatterer. Due to the reversal of the sign of the complex exponential phase factor, this latter term can be interpreted as a mirror image of the Rayleigh scatterer sitting beneath the substrate with an internal electric field strength determined by the Fresnel reflection coefficient. Within the Born Approximation (that is, low permittivity contrast), this first-order image term dominates the interaction between Rayleigh scatterer and substrate. Higher-order multiple scattering effects between the Rayleigh object and substrate can be ignored. Similarly, multiple

scattering effects between particles lying on the substrate can also be neglected due to the assumed low permittivity contrast. The volume integrals of (10) and (11) can therefore be evaluated by simply integrating over the entire volume of the Rayleigh object distribution. Thus, (10) and (11) are now evaluated as follows.

From Figure 1, we have the following relationship between position vectors, $\mathbf{R} = \mathbf{R_0} - \mathbf{r}$. Therefore, the distance R between a source point inside the Rayleigh object and the field point at P is given by $R = \sqrt{R_0^2 + r^2 - 2\mathbf{R_0} \cdot \mathbf{r}}$. Under the assumed far-field conditions we have $R_0 \gg r$, so that a binomial expansion of the above square root gives the following far-field approximation for R:

$$R \cong R_0 - \hat{\mathbf{R}}_\mathbf{0} \cdot \mathbf{r} \tag{12}$$

Substituting for R using (12) in the defining expression for the scalar Green's function ϕ then gives:

$$\phi = \frac{e^{-ik_1 R}}{R} \cong \frac{e^{-ik_1 R_0}}{R_0} e^{+ik_1 \hat{\mathbf{R}}_\mathbf{0} \cdot \mathbf{r}} \tag{13}$$

The scalar product in (13) is given by the following explicit expression:

$$\hat{\mathbf{R}}_\mathbf{0} \cdot \mathbf{r} = x \sin\theta_i \cos\phi_i + y \sin\theta_i \sin\phi_i + z \cos\theta_i \tag{14}$$

In the integrands of (10) and (11) we have the product $\phi\phi_t$ which, using the results of (13), (14) and (7), can now be expressed as:

$$\begin{aligned} \phi\phi_t &\cong \frac{e^{-jk_1 R_0}}{R_0} e^{+jk_1 (x \sin\theta_i \cos\phi_i + y \sin\theta_i \sin\phi_i + z \cos\theta_i)} \\ &\quad e^{-jk_1 (x \sin\theta_i \cos\phi_i + y \sin\theta_i \sin\phi_i)} \\ &= \frac{e^{-jk_1 R_0}}{R_0} e^{jk_1 z \cos\theta_i} \end{aligned} \tag{15}$$

Substituting (15) into (10) gives for perpendicular polarization:

$$E_s^V = \frac{k_0^2}{4\pi} (\varepsilon - \varepsilon_1) E_0 \frac{e^{-jk_1 R_0}}{R_0} \int\limits_V \left(e^{2jk_1 z \cos\theta_i} + r_s^{12} \right) dV \tag{16}$$

Writing the volume element $dV = dSdz$, and introducing the effective height, d, and surface area, Σ, for the Rayleigh scatterers, the integral in (16) is evaluated as follows:

$$\begin{aligned} \int\limits_V \left(e^{2jk_1 z \cos\theta_i} + r_s^{12} \right) dV &= \iint\limits_\Sigma dS \int\limits_0^d e^{2jk_1 z \cos\theta_i} dz + r_s^{12} \iint\limits_\Sigma dS \int\limits_0^d dz \\ &= \Sigma d \left(e^{jk_1 d \cos\theta_i} \mathrm{sinc}\,(k_1 d \cos\theta_i) + r_s^{12} \right) \end{aligned} \tag{17}$$

The product Σd is equivalent to the volume of the object, V. Since $k_1 d \ll 1$, the *sinc* function in (17) is well-approximated by unity. Therefore, the following result for perpendicular polarization is obtained using the result of (17) in (16):

$$E_s^V = \frac{k_0^2}{4\pi}(\varepsilon - \varepsilon_1) E_0 \frac{e^{-jk_1 R_0}}{R_0} \Sigma d \left\{ e^{jk_1 d\cos\theta_i} + r_s^{12} \right\} \tag{18}$$

A similar analysis can be applied to (11) for parallel polarization giving the following result

$$E_p^V = \frac{k_0^2}{4\pi}(\varepsilon - \varepsilon_1) E_0 \frac{e^{-jk_1 R_0}}{R_0} \Sigma d \left\{ \cos 2\theta_i e^{jk_1 d\cos\theta_i} + r_p^{12} \right\} \tag{19}$$

It now remains to determine the surface integral contribution to the scattered field as per Equation (3) which is repeated below:

$$\mathbf{E}_{\text{scat}}^S = \frac{-j}{4\pi\omega\varepsilon_0\varepsilon_1} \iint\limits_S \left[(\mathbf{J}_s \cdot \nabla) \nabla\phi + k_1^2 \mathbf{J}_s \phi - j\omega\varepsilon_0\varepsilon_1 \mathbf{M}_s \times \nabla\phi \right] dS$$

On performing the necessary vector differential operations as before, the above integral becomes:

$$\mathbf{E}_{\text{scat}}^S = \frac{-jk_1}{4\pi} \iint\limits_S \left[aZ_1 \mathbf{J}_s + bZ_1 \left(\mathbf{J_s} \cdot \hat{\mathbf{R}} \right) \hat{\mathbf{R}} + c\mathbf{M}_s \times \hat{\mathbf{R}} \right] \phi \, dS \tag{20}$$

where in (20) a and b are defined as before (see Equation (8)) and $c = 1 - \frac{j}{k_1 R}$. Also, in (20), we have

Z_1 = Intrinsic impedance of host medium = Z_0/n_1

Z_0 = Impedance of free-space = 376.73Ω

n_1 = Refractive index of host medium.

For large $k_1 R$, $a \approx 1$, $b \approx -1$ and $c \approx 1$ so that (20) becomes

$$\mathbf{E}_{\text{scat}}^S = \frac{-jk_1}{4\pi} \iint\limits_S \mathbf{Q} \, \phi \, dS \tag{21}$$

where in (21)

$$\mathbf{Q} = Z_1 \mathbf{J}_s - Z_1 \left(\mathbf{J_s} \cdot \hat{\mathbf{R}} \right) \hat{\mathbf{R}} + \mathbf{M}_s \times \hat{\mathbf{R}} \tag{22}$$

The equivalent electric and magnetic currents on the substrate surface, $\mathbf{J}_s$ and $\mathbf{M}_s$, respectively, are defined in terms of the tangential field components as follows:

$$\begin{aligned} Z_1 \mathbf{J}_s &= Z_1 \hat{\mathbf{n}} \times \mathbf{H} \equiv \hat{\mathbf{z}} \times \left[\hat{\mathbf{k}}_\mathbf{i} \times \mathbf{E_{inc}} + \hat{\mathbf{k}}_\mathbf{r} \times \mathbf{E_{ref}} \right] \\ \mathbf{M_s} &= \mathbf{E} \times \hat{\mathbf{n}} \equiv \mathbf{E_{inc}} \times \hat{\mathbf{z}} + \mathbf{E_{ref}} \times \hat{\mathbf{z}} \end{aligned} \tag{23}$$

In the above definitions, $\hat{\mathbf{n}}$ is a unit normal vector on the substrate surface pointing into the host medium ($= \hat{\mathbf{z}}$). Using (5), the incident electric field is $\mathbf{E}_{\text{inc}} = E_0\phi_{\text{inc}}\left(\cos\gamma\hat{\mathbf{s}} + \sin\gamma\hat{\mathbf{p}}_i\right)$ and the reflected electric field is $\mathbf{E}_{\text{ref}} = E_0\phi_{\text{ref}}\left(r_s^{12}\cos\gamma\hat{\mathbf{s}} + r_p^{12}\sin\gamma\hat{\mathbf{p}}_r\right)$. Substituting (23) into (22) and setting $\hat{\mathbf{R}} \approx \hat{\mathbf{R}}_{\mathbf{0}}$ for far-field conditions eventually results in the following expressions for (21) for perpendicular and parallel polarization, respectively

$$E_s^S = \mathbf{E}_{\mathbf{scat}}^{\mathbf{S}}.\hat{\mathbf{s}} = \frac{jk_1}{2\pi}\cos\theta_i E_0 r_s^{12}\iint\limits_S \phi_{\text{ref}}\,\phi\,dS \tag{24}$$

$$E_p^S = \mathbf{E}_{\mathbf{scat}}^{\mathbf{S}}.\hat{\mathbf{p}}_r = \frac{jk_1}{2\pi}\cos\theta_i E_0 r_p^{12}\iint\limits_S \phi_{\text{ref}}\,\phi\,dS \tag{25}$$

Equations (24) and (25) are consistent with the well-known Physical Optics approximation.

The common integrand in (24) and (25) contains the product $\phi_{\text{ref}}\phi$. Using the definition of ϕ_{ref} given in (6) and the far-field approximation of the scalar Green's function ϕ given in (13) gives the following result

$$\begin{aligned}\phi_{\text{ref}}\phi &\cong \frac{e^{-jk_1R_0}}{R_0}e^{+jk_1\hat{\mathbf{R}}_{\mathbf{0}}\cdot\mathbf{r}}e^{-jk_1(x\sin\theta_i\cos\phi_i + y\sin\theta_i\sin\phi_i + z\cos\theta_i)} \\ &\equiv \frac{e^{-jk_1R_0}}{R_0}\end{aligned} \tag{26}$$

Therefore, using (26) in (24) and (25) gives

$$E_s^S = \frac{jk_1}{2\pi}\cos\theta_i E_0 r_s^{12}\frac{e^{-jk_1R_0}}{R_0}S \tag{27}$$

$$E_p^S = \frac{jk_1}{2\pi}\cos\theta_i E_0 r_p^{12}\frac{e^{-jk_1R_0}}{R_0}S \tag{28}$$

where in the above, S is the surface area of the substrate.

The total scattered field for perpendicular polarization is then given by the sum of (18) and (27) which can be expressed in the following form:

$$\begin{aligned}&E_s = E_s^S + E_s^V \\ &= \frac{jk_1}{2\pi}\frac{e^{-jk_1R_0}}{R_0}S\cos\theta_i E_0\left[r_s^{12} - \frac{jk_0^2 d\alpha}{2k_1\cos\theta_i}(\varepsilon - \varepsilon_1)\left\{e^{jk_1 d\cos\theta_i} + r_s^{12}\right\}\right]\end{aligned} \tag{29}$$

In (29), the fraction of the surface area covered by the Rayleigh scatterers is defined by the dimensionless parameter, $\alpha = \frac{\Sigma}{S}$.

For parallel polarization, the result for the total scattered field is found from the sum of (19) and (28), namely

$$E_p = E_p^S + E_p^V = \frac{jk_1}{2\pi}\frac{e^{-jk_1R_0}}{R_0} S\cos\theta_i E_0 \left[r_p^{12} - \frac{jk_0^2 d\alpha}{2k_1\cos\theta_i}(\varepsilon-\varepsilon_1)\left\{\cos 2\theta_i e^{jk_1 d\cos\theta_i} + r_p^{12}\right\}\right] \quad (30)$$

Therefore, for the case of a distribution of Rayleigh objects lying above the substrate, the complex ellipticity ratio ρ^{12} is defined as follows:

$$\rho^{12} = \frac{E_p}{E_s} = \frac{\text{Total scattered field for parallel polarization}}{\text{Total scattered field for perpendicular polarization}}$$

The superscript '12' is used in the above to denote an incident wave residing in the host medium (that surrounding the Rayleigh object = medium '1') impinging on the substrate (= medium '2').

Substituting (29) and (30) into the above gives

$$\rho^{12} = \frac{r_p^{12} - jA^{12}\left\{\cos 2\theta_i e^{j\delta_{12}} + r_p^{12}\right\}}{r_s^{12} - jA^{12}\left\{e^{j\delta_{12}} + r_s^{12}\right\}} \quad (31)$$

In (31), the parameters A^{12} and δ_{12} are defined as follows

$$A^{12} = \frac{k_0^2 d\alpha}{2k_1\cos\theta_i}(\varepsilon - \varepsilon_1) \qquad \delta_{12} = k_1 d\cos\theta_i$$

For reflectivity, r^{12}, the parameter of interest is that pertaining to parallel polarization only which, using the result of (30) becomes

$$r^{12} = \left|r_p^{12} - jA^{12}\left\{\cos 2\theta_i e^{j\delta_{12}} + r_p^{12}\right\}\right|^2 \quad (32)$$

Equations (31) and (32) are the salient results for the ellipticity ratio and reflectivity arising from the integral equation analysis described for the case of a distribution of Rayleigh objects residing on a substrate.

The following section concerns the case where the Rayleigh objects reside beneath the substrate. It is this latter case that is compared with previously published measured results for the ellipticity ratio and reflectivity.

2.2. Object Beneath Substrate

Figure 2 shows a similar configuration to that presented in Subsection 2.1 except that the Rayleigh object now lies beneath the substrate. In this case, the substrate material is assumed to be largely transparent thereby permitting incident light to illuminate the object via the substrate-host medium interface.

Thus, the incident light originates from within the substrate medium with permittivity ε_2. Similarly, the scattered field at the point P also lies within the semi-infinite substrate medium. The analysis for the scattered field at P proceeds as before, with the evaluation of a volume integral term involving the induced polarization current density within the Rayleigh object, and a surface integral term involving the equivalent electric and magnetic surface currents on the interface surface S.

The surface integral contribution to the scattered field is identical in mathematical form to the previous case with the object located above the substrate except for the interchange of incident and host media. This contribution gives rise to the Physical Optics results given in Equations (24) and (25). Evaluation of the volume integral contribution to the scattered field for the case of the Rayleigh object lying beneath the substrate requires a slight modification to the analysis described before which is as follows.

With the Rayleigh object beneath the substrate, application of the Born Approximation in this instance means that the total electric field inside the Rayleigh object is that due to the refracted plane-wave in the host medium with the object assumed to be absent. This is

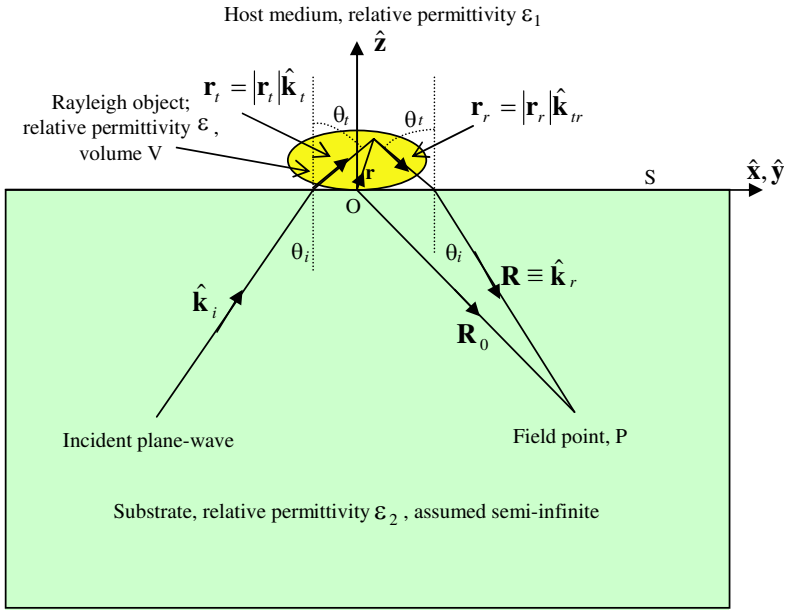

Figure 2. Geometry of a Rayleigh object beneath a substrate.

found simply by multiplying the incident field from within the substrate medium by the appropriate Fresnel transmission coefficient for the planar interface. Therefore, analogous to Equation (5), we have for the total electric field in the Rayleigh object volume:

$$\mathbf{E}_{\text{total}} \cong E_0 \phi_{\text{trans}} \left(t_s^{21} \cos\gamma \hat{\mathbf{s}} + t_p^{21} \sin\gamma \hat{\mathbf{p}}_t \right) \tag{33}$$

In Equation (33)

$\hat{\mathbf{s}}$ = Unit vector perpendicular to the plane of incidence.

$\hat{\mathbf{p}}_t$ = Unit vector parallel to the plane of incidence for the refracted wave = $\hat{\mathbf{k}}_t \times \hat{\mathbf{s}}$.

$\hat{\mathbf{k}}_t$ = Unit propagation vector for refracted wave in host medium.

t_s^{21} = Fresnel transmission coefficient for perpendicular polarization with incident field in medium '2, refracted field in medium '1'.

t_p^{21} = Fresnel transmission coefficient for parallel polarization with incident field in medium '2, refracted field in medium '1'.

ϕ_{trans} = Phase factor for the plane-wave transmitted into the Rayleigh object.

In order to resolve the scattered field at the field point P into parallel and perpendicularly polarized components, we must first identify the contribution from the volume integral that gives rise to a plane-wave propagating in the specularly reflected direction denoted by the unit vector $\hat{\mathbf{k}}_r$. From the geometry shown in Figure 2, a plane wave scattered in the direction given by the unit vector $\hat{\mathbf{k}}_{tr}$ will be refracted at the substrate interface and emerge parallel to the vector $\hat{\mathbf{k}}_r$. Analogous to the above-substrate case, we also need to define a unit vector $\hat{\mathbf{p}}_{tr} = -\hat{\mathbf{k}}_{tr} \times \hat{\mathbf{s}}$ for the parallel-polarized field component radiated into the host medium by the induced polarization current inside the Rayleigh object. Note that the volume integral formulation given previously determines the scattered field at a point lying within the host medium. In order to determine the scattered field at the point P in the substrate medium, it is therefore necessary to multiply the scattered field so determined by the appropriate Fresnel transmission coefficient for a wave refracted into the substrate medium. Therefore, making similar far-field approximations for the phase factors as before, we obtain the following volume integrals:

For perpendicular polarization

$$E_s^V \,|_{21} = \mathbf{E}_{\text{scat}}^V \cdot \hat{\mathbf{s}} = \frac{k_0^2}{4\pi} (\varepsilon - \varepsilon_1) E_0 \frac{e^{-jk_2 R_0}}{R_0} t_s^{12} t_s^{21} \int\limits_V e^{2jk_1 z \cos\theta_t} \, dV \tag{34}$$

For parallel polarization

$$E_p^V\,|_{21} = \mathbf{E}_{\text{scat}}^V \cdot \hat{\mathbf{p}}_{tr}$$
$$= \frac{k_0^2}{4\pi}\,(\varepsilon - \varepsilon_1)\,E_0 \frac{e^{-jk_2R_0}}{R_0} t_p^{12} t_p^{21} \int\limits_V \cos 2\theta_t e^{2jk_{1z}\cos\theta_t}\,dV \quad (35)$$

where for parallel polarization, the term $\cos 2\theta_t$ arises from the scalar product $\hat{\mathbf{p}}_t \cdot \hat{\mathbf{p}}_{tr}$ and the terms t_s^{12} and t_p^{12} are the Fresnel transmission coefficients for perpendicular and parallel polarization, respectively, for plane waves refracted into medium '2' from an incident wave in medium '1' (see Appendix).

The relevant surface integral terms for the Rayleigh object lying beneath the substrate are

$$E_s^S\,|_{21} = \frac{jk_2}{2\pi}\cos\theta_i E_0 r_s^{21} \frac{e^{-jk_2R_0}}{R_0} S \quad (36)$$

$$E_p^S\,|_{21} = \frac{jk_2}{2\pi}\cos\theta_i E_0 r_p^{21} \frac{e^{-jk_2R_0}}{R_0} S \quad (37)$$

where k_2 is the propagation constant for medium '2'.

Evaluating the volume integrals in (34) and (35) in the same way as for the above-substrate case, and adding the surface integral terms of (36) and (37) gives the following expressions for the ellipticity ratio ρ^{21}

$$\rho^{21} = \frac{r_p^{21} - jt_p^{12}t_p^{21}A^{21}e^{-j\delta_{21}}\cos 2\theta_t}{r_s^{21} - jt_s^{12}t_s^{21}A^{21}e^{-j\delta_{21}}} \quad (38)$$

In (38), the parameters A^{21} and δ_{21} are defined as follows

$$A^{21} = \frac{k_0^2 d\alpha}{2k_2\cos\theta_t}\,(\varepsilon - \varepsilon_1) \qquad \delta_{21} = k_1 d\cos\theta_t$$

For the reflectivity, r^{21} (parallel polarization only) the result is

$$r^{21} = \left| r_p^{21} - jt_p^{12}t_p^{21}A^{21}e^{-j\delta_{21}}\cos 2\theta_t \right|^2 \quad (39)$$

3. COMPARISON WITH MEASURED DATA

The expressions for the ellipticity ratio given in (31) and (38) are of a simple, closed form that offers computational simplifications for effective height and surface coverage of adsorbed particles on or beneath a substrate. This is in contrast to previously published formulae associated with thin-island film theory [1, 2] and with rigorous spherical harmonic scattering models for spheres [3–5]. To validate the accuracy of the formulation derived in this paper, a comparison

was made with previously published measured data for ellipticity ratio and reflectivity. A suitable set of data for comparison is that due to van Duijvenbode & Koper [6] for the case of latex spheres of various known radii immersed in water above a glass substrate. This case corresponds to that for which the Rayleigh objects are lying beneath the substrate layer so that Equations (38) and (39) are the relevant theoretical expressions to be used for the ellipticity ratio and reflectivity, respectively.

From the experiments described in [6], layers of latex spheres with known nominal radii of 10 nm, 30 nm and 50 nm were considered. Plane-wave illumination with a free-space wavelength of 632.8 nm was used with measurements of ellipticity ratio and reflectivity made in the vicinity of the Brewster angle. The surface coverage of the adsorbed latex spheres was not known a priori in the experiments reported in [6] but was estimated from the ellipticity ratio and reflectivity data using a number of different models (Abeles matrix and optical invariants). The refractive index parameters of the (lossless) materials used in these experiments are given below along with the relative permittivity (equal to the square of refractive index):

Latex spheres: Refractive index, $n = 1.591$, $\varepsilon = 2.531$.

Glass substrate: Refractive index, $n_2 = 1.515$, $\varepsilon_2 = 2.295$.

Water host medium: Refractive index, $n_1 = 1.333$, $\varepsilon_1 = 1.777$.

The Brewster angle, θ_B, for the above material configuration is given by $\theta_B = \tan^{-1}\left(\frac{n_1}{n_2}\right) = 41.34^\circ$.

The modulus and phase of the ellipticity ratio were evaluated using Equation (38) for incidence angles a few degrees either side of the Brewster angle using the effective height, d, and surface coverage, α, as variable parameters. Similarly, reflectivity data was evaluated using Equation (39).

The values of surface coverage and effective height parameters were adjusted to obtain the best fit to the measured values reported in [6]. It was found that by varying the values of d and α to obtain the observed angular location and value of the minimum modulus, a good fit could be obtained between theory and measurement over the full range of incidence angles measured for both modulus and phase of the ellipticity ratio.

Figures 3, 4 and 5 plot the measured and best-fit theoretical results for the modulus and phase of the ellipticity ratio and reflectivity for latex spheres of nominal radii 10 nm, 30 nm and 50 nm, respectively. Figures denoted by suffix 'a' show the modulus of ellipticity ratio, suffix 'b' the phase of the ellipticity ratio, and suffix 'c' the reflectivity data.

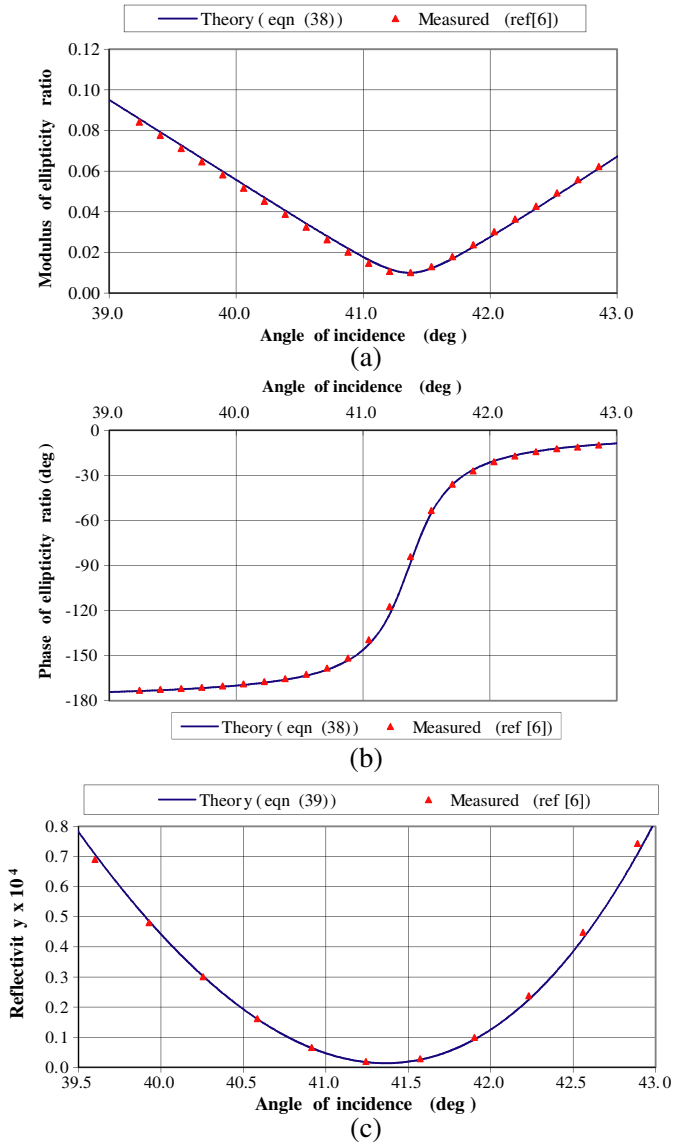

Figure 3. (a) Modulus of ellipticity ratio for latex spheres of nominal radius 10 nm. The theoretical curve uses an effective radius of 10 nm and a surface coverage of 15.0%. (b) Phase of ellipticity ratio for latex spheres of nominal radius 10 nm. The theoretical curve uses an effective radius of 10 nm and a surface coverage of 15.0%. (c) Reflectivity for latex spheres of nominal radius 10 nm. The theoretical curve uses an effective radius of 10 nm and a surface coverage of 14.0%.

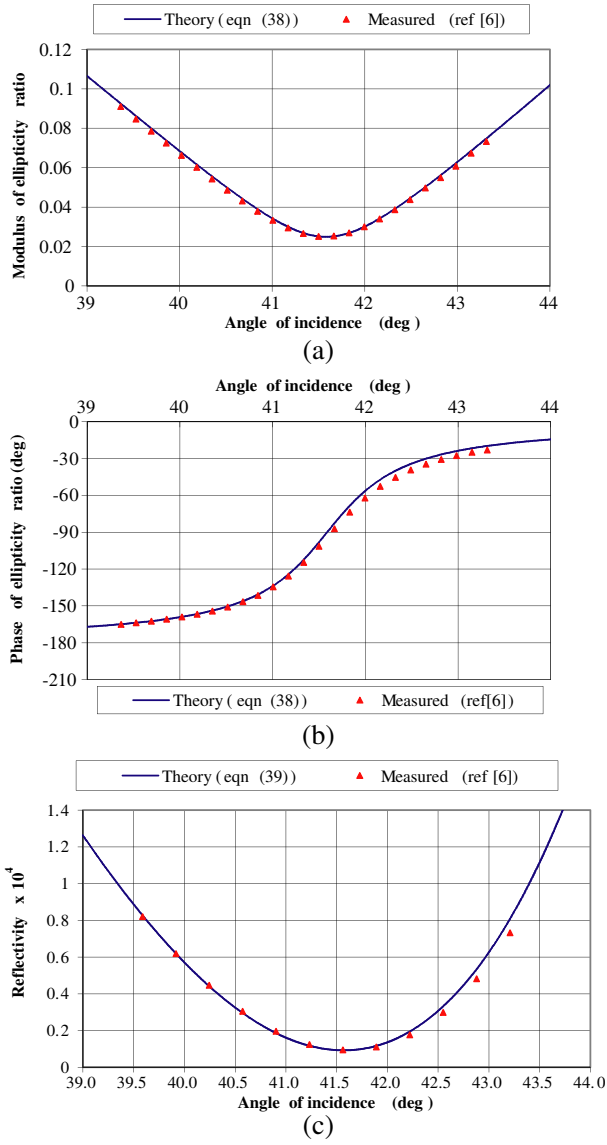

Figure 4. (a) Modulus of ellipticity ratio for latex spheres of nominal radius 30 nm. The theoretical curve uses an effective radius of 32 nm and a surface coverage of 12.0%. (b) Phase of ellipticity ratio for latex spheres of nominal radius 30 nm. The theoretical curve uses an effective radius of 32 nm and a surface coverage of 12.0%. (c) Reflectivity for latex spheres of nominal radius 30 nm. The theoretical curve uses an effective radius of 32 nm and a surface coverage of 12.0%.

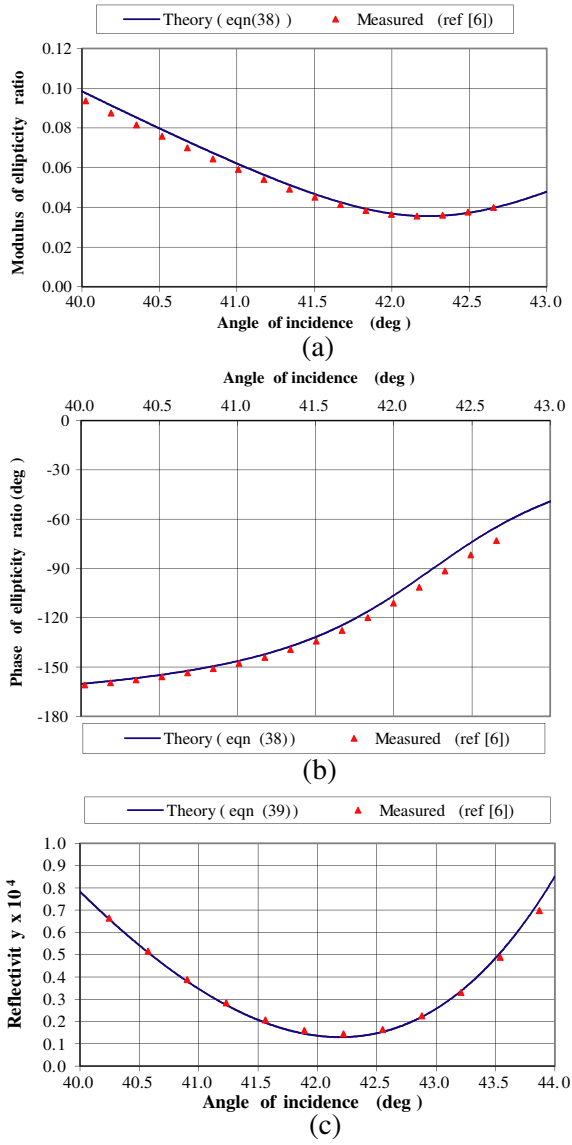

Figure 5. (a) Modulus of ellipticity ratio for latex spheres of nominal radius 50 nm. The theoretical curve uses an effective radius of 59 nm and a surface coverage of 10.0%. (b) Phase of ellipticity ratio for latex spheres of nominal radius 50 nm. The theoretical curve uses an effective radius of 59 nm and a surface coverage of 10.0%. (c) Reflectivity for latex spheres of nominal radius 50 nm. The theoretical curve uses an effective radius of 59 nm and a surface coverage of 10.0%.

It should be noted that in making the comparison between the theoretical results obtained using Equations (38) and (39) and the measured values reported in [6], the sign and sense of the phase of the theoretical ellipticity ratio had to be modified to be consistent with that shown in the measured data. This is due to the conventions used in the respective analyses and is discussed in Appendix A.

The computed values of d and α obtained from the optical measurements and theories reported in [6] were compared with those using the theory described in this paper. The results are summarised in Table 1. In this table, the effective radii values shown are one half of the effective height, d.

Table 1. Calculated effective and true radii, and theoretical percentage surface coverage (in parentheses) as obtained from the theory described in this paper, and from the Abeles matrix and optical invariants methods described in [6].

True radius (nm)	This paper Ellipso-metry	This paper Reflect-ometry	Abeles matrix [6] Ellipso-metry	Abeles matrix [6] Reflect-ometry	Optical invariants [6] Ellipso-metry	Optical invariants [6] Reflect-ometry
10 ± 2	10 (15%)	10 (14%)	8 (18%)	9 (20%)	10 (14%)	12 (19%)
30 ± 3	32 (12%)	32 (12%)	37 (13%)	36 (13%)	37 (14%)	35 (15%)
50 ± 2	59 (10%)	59 (10%)	58 (13%)	58 (13%)	53 (14%)	50 (16%)

The results shown in Table 1 indicate that the effective radii and surface coverage values obtained from the theory described in this paper are very consistent between the ellipticity ratio and reflectometry models used. The effective radii for the 10 nm and 30 nm latex spheres are recovered very accurately from either of Equations (38) or (39), with calculated values lying within the measured dimensional tolerance. Overall, the theory described in this paper determines effective radii for the 10 nm and 30 nm spheres more accurately than the Abeles matrix and optical invariants methods. Values obtained for the largest sphere (nominal radius 50 nm) are over-estimated and lie outside the dimensional tolerance, with the exception of the optical invariants result using reflectometry. One possible explanation is that

the size of the latex spheres in this case may not be small enough with respect to the wavelength in the host medium for the theory to be accurate.

As for the surface coverage values obtained, there was no 'ground truth' data available from the experiments reported in [6] to enable direct validation with theoretical values. In general, surface coverage values obtained from the theory described in this paper are typically lower than those obtained from the Abeles matrix and optical invariants methods. This result appears to be consistent with the observations of Wormeester et al. [9]. In [9], it was reported that below surface coverage values of 20%, the thin-island film theory tended to over-estimate the surface coverage obtained from ellipsometry data unless details of the lateral distribution of the particles was available.

4. CONCLUSIONS

Within the restrictions of the Rayleigh region and Born Approximation, simple expressions for the ellipticity ratio and reflectivity of a layer of adsorbed particles on or beneath a dielectric substrate were derived using fundamental surface and volume integral expressions for the scattered electric field. With these approximations in place, the resulting expressions for the ellipticity ratio and reflectivity are independent of the particle shape, and do not rely on an analysis of dielectric spheres unlike the widely used thin-island film theory.

The theory described in this paper automatically models a first-order representation of the image dipole contribution to the scattered field but does not include higher-order particle-substrate interactions or interactions between particles. Nevertheless, results obtained with the theory described agree well with measured data for low-contrast Rayleigh objects. With the aforementioned in mind, the expressions derived in this paper should provide an accurate description of polarized scattered light from adsorbed layers consisting typically of biological materials on or beneath dielectric substrates.

ACKNOWLEDGMENT

The author would like to offer his sincere thanks to Dr. Rene van Duijvenbode, formerly of Leiden University, The Netherlands, for kindly making available his measured data in tabular form for use in this paper. The author would also like to thank Dr Mark Clarkson of IRL and Andres Pantoja of Beaglehole Instruments Ltd for their constructive comments and feedback. The work described in this paper was supported by funding from the New Zealand Ministry of Science and Innovation, contract number C08X0708.

APPENDIX A. A NOTE ON FRESNEL REFLECTION COEFFICIENTS AND SIGN CONVENTIONS USED FOR THE COMPLEX ELLIPTICITY RATIO

Expressions for the Fresnel reflection and transmission coefficients used in this paper and in Equations (1) and (2) of reference [6], which was used as a source of measured data, are given below:

$$r_s^{12} = \frac{n_2\cos\theta_t - n_1\cos\theta_i}{n_2\cos\theta_t + n_1\cos\theta_i} \qquad r_p^{12} = \frac{n_2\cos\theta_i - n_1\cos\theta_t}{n_2\cos\theta_i + n_1\cos\theta_t} \quad \text{(A1)}$$

$$t_s^{12} = \frac{2n_1\cos\theta_i}{n_2\cos\theta_t + n_1\cos\theta_i} \qquad t_p^{12} = \frac{2n_1\cos\theta_i}{n_1\cos\theta_t + n_2\cos\theta_i} \quad \text{(A2)}$$

In (A1) and (A2) above, light is incident from medium '1' with refractive index n_1 and angle of incidence θ_i. Light is refracted into medium '2' with refractive index n_2 and refraction angle θ_t. Plane-wave reflection coefficients are designated by r_s^{12} and r_p^{12}, and transmission coefficients by t_s^{12} and t_p^{12}. The subscripts 's' and 'p' refer to perpendicular and parallel polarized light, respectively.

The mathematical behaviour of the equations for the reflection coefficients in (A1) can be used to determine how the phase of the ellipticity ratio should behave at the extremes of incidence angle and as the transition through the Brewster angle occurs. The measured results for the phase of ellipticity ratio, Δ, that appear in Figure 4 of reference [6], show curves for latex spheres of various radii but also a curve for the Fresnel case, that is, with just the dielectric interface and no adsorbed particles present.

This measured result for the Fresnel case passes through a value of negative 90° as the angle of incidence transits the Brewster angle. At smaller incidence angles, the value tends to negative 180° (as normal incidence is approached), and approaches a value of zero at larger incidence angles (towards grazing incidence). However, these limiting values, and that at the Brewster angle itself, are inconsistent with the reflection coefficient equations in (A.1). To illustrate this, consider the case of normal incidence for which $\theta_i = \theta_t = 0$.

One obtains $r_s^{12} = r_p^{12} = \frac{n_2 - n_1}{n_2 + n_1}$. Therefore, the corresponding ellipticity ratio for this limiting case is $\frac{r_p^{12}}{r_s^{12}} = 1$. This is purely real with the respective reflection coefficients in phase; that is, a phase angle of zero, not negative 180°as shown in Figure 4 of reference [6]. Similarly, as we approach grazing incidence, for which $\theta_i = 90°$, we have $\cos\theta_i = 0$ and therefore $r_s^{12} = 1$ and $r_p^{12} = -1$. Thus, the respective reflection coefficients are now in anti-phase giving a value of negative 180° for the ellipticity ratio at grazing incidence. This is in contrast to the value of zero given in Figure 4 of reference [6].

The above analysis highlights a discrepancy in the phase angle of the ellipticity ratio between the measured results of [6] and the values expected from the Fresnel reflection coefficient equations used in the analysis of this paper and that of [6]. Therefore, when comparing the predicted values of the ellipticity ratio phase derived in this paper with the measured values, the sign and sense of the phase angle of the predicted results was amended to be consistent with that of the measured results of [6]. This allowed direct comparison to be made between theory and experiment despite the difference in sign convention suspected in the sign and sense of the measured ellipticity ratio phase angle.

REFERENCES

1. Bedeaux, D. and J. Vlieger, "A phenomenological theory of the dielectric properties of thin films," *Physica*, Vol. 67, 55–73, 1973.
2. Vlieger, J. and D. Bedeaux, "A statistical theory for the dielectric properties of thin-island films," *Thin Solid Films*, Vol. 69, 107–130, 1980.
3. Bobbert, P. A. and J. Vlieger, "Light scattering by a sphere on a substrate," *Physica*, Vol. 137A, 209–242, 1986.
4. Bobbert, P. A., J. Vlieger, and R. Greef, "Light reflection from a substrate sparsely seeded with spheres — Comparison with an ellipsometric experiment," *Physica*, Vol. 137A, 243–257, 1986.
5. Videen, G., "Light scattering from a sphere behind a surface," *Journal of the Optical Society of America A*, Vol. 10, No. 1, 110–117, 1993.
6. Van Duijvenbode, R. C. and G. J. M. Koper, "A comparison between light reflectometry and ellipsometry in the Rayleigh regime," *Journal of Physical Chemistry B*, Vol. 104, No. 42, 9878–9886, 2000.
7. Moreno, F., J. M. Saiz, and F. González, "Light scattering by particles on substrates. Theory and experiments," *Light Scattering and Nanoscale Surface Roughness*, edited by Maradudin, A. A., 305–340, Springer, New York, 2007.
8. Stratton, J. A. and L. J. Chu, "Diffraction theory of electromagnetic waves," *Physical Review*, Vol. 56, 99–107, 1939.
9. Wormeester, H., E. S. Kooij, and B. Poelsema, "Unambiguous optical characterisation of nanocolloidal gold films," *Physical Review B*, Vol. 68, 085406-1–6, 2003.